

## Atomic Radial Distributions and Ion-Ion Potential in Liquid Gallium\*

P. ASCARELLI

*Comitato Nazionale per l'Energia Nucleare, C.C.R. Euratom, Ispra, Varese, Italy*

(Received 19 August 1965)

The atomic radial distributions for liquid gallium at 50 and 150°C have been derived from the measured neutron-diffraction intensity patterns. In this study the fundamental equation of the Percus—Yevick (PY) theory of liquids has been set out in a simple form suitable for the direct exploitation of neutron-diffraction data. Equivalent forms of the (PY) equation have been obtained. An approximate form of the ion-ion interaction in liquid gallium at 50 and 150°C has been derived. Analogies in the atomic short-range order have been found between the liquid phase and the solid metastable phase  $\beta$ . These analogies are stressed by the changes in the density and in the resistivity of the metastable phase  $\beta$  at melting point; the behavior displayed is common to the majority of metals.

### SECTION 1

#### 1.1 INTRODUCTION

IN the last few years much theoretical effort has been devoted to the molecular theories of liquids<sup>1</sup> and to the electronic properties of liquid metals.<sup>2</sup>

Gallium is an interesting element because of its anomalous behavior in melting. Among its other well-known features—for example, the increase in density from solid to liquid phase at melting point—we should point out the recent discovery of two solid phases metastable at normal pressure.<sup>3</sup> These metastable phases, named  $\beta$  and  $\gamma$ , melt at  $-16.3$  and  $-35.6^\circ\text{C}$ , respectively, and have densities higher than the liquid phase (undercooled) at the same temperature.<sup>4</sup> Moreover, work on positron annihilation<sup>5,6</sup> suggests directly a change in the electronic structure at melting, whereas measurements of electronic transport properties<sup>7</sup> point out difficulties in the interpretation of liquid-phase experimental data.

In this work, neutron diffraction is used to determine the structure of liquid gallium at two temperatures (50 and 150°C). A comparison is made with previous x-ray<sup>8,9</sup> and electron-diffraction<sup>10</sup> studies. Finally, the liquid structure has been compared with that of solid stable and metastable phases.<sup>11</sup>

In this study, an attempt is made (in the wave-vector space) to exploit the Percus-Yevich (PY) approximation in the theory of liquids,<sup>12</sup> in order to

obtain an effective ion-ion potential in liquid gallium from neutron-diffraction intensity data.

Apart from any plausible approximation involved in the (PY) theory of liquids or in its exploitation for a liquid metal, it must be admitted that at this stage it is rather idealistic to expect more than a qualitative result by this kind of approach, especially for metallic systems (where long-range interactions are predicted), mainly because of experimental difficulties in small-angle neutron scattering. This question will be discussed further in this study.

#### 1.2 EXPERIMENTAL PROCEDURES

Neutrons of wavelength  $\lambda=0.905$  Å were selected from a beam of neutrons from the CP-5 Ispra 1 reactor, operated at a power of 5 MW by reflection from the {111} planes of aluminum single crystal. The spectrometer used has been described previously.<sup>13</sup> The liquid gallium was put into a very thin-walled cylindrical quartz container (17 cm high and 0.9 cm diameter) chosen in order to obtain a good compromise between the scattered intensity and the level of multiple scattering.

The container was supported and surrounded by two cylindrical pieces of copper which were heated by two electrically isolated heaters in parallel connection, and set vertically at a distance of 6 cm from one another. The upper heater was supported by a very thin-walled aluminum cylinder (3.4 cm diam), which also acted as thermal screening between the gallium sample and the atmosphere. Hence the impinging and scattered neutron beams (5 cm high, 2 cm wide) passed into and out of the quartz container only through this thin aluminum cylinder. During the experiment the temperature of the sample was continuously registered using as a sensing element an iron-constantan thermocouple threaded through a thin Pyrex capillary tube closed at one end.

A drop of mercury was placed at the extremity of the capillary tube in order to ensure good thermal contact between the joint of the thermocouple and the wall of

\* Preliminary results of this paper were communicated at the "L. Congresso Nazionale di Fisica" in Catania, 1964 (unpublished).

<sup>1</sup> J. S. Rowlinson, *Cont. Phys.* **5**, 359 (1964).

<sup>2</sup> N. E. Cusack, *Rept. Progr. Phys.* **26**, 361 (1963).

<sup>3</sup> L. Bosio and A. Defrain, *J. Chim. Phys.* **61**, 859 (1964).

<sup>4</sup> L. Bosio, *Compt. Rend.* **259**, 4545 (1964).

<sup>5</sup> A. T. Stewart, J. H. Kusmiss, and J. H. March, *Phys. Rev.* **132**, 495 (1963).

<sup>6</sup> D. R. Gustafson and A. R. Mackintosh, *Phys. Letters* **5**, 234 (1963).

<sup>7</sup> N. E. Cusack, P. W. Kendall, and A. S. Marwaha, *Phil. Mag.* **7**, 1745 (1962).

<sup>8</sup> H. Menke, *Z. Physik* **33**, 593 (1932).

<sup>9</sup> H. Hendus, *Z. Naturforsch.* **2a**, 505 (1947).

<sup>10</sup> H. Richter and S. Steeb, *Z. Metallk.* **7**, 369 (1959).

<sup>11</sup> H. Curien, E. Rimsky, and A. Defrain, *Bull. Soc. Franc. Mineral. Crist.* **84**, 260 (1961).

<sup>12</sup> J. K. Percus and G. J. Yevick, *Phys. Rev.* **110**, 1 (1958).

<sup>13</sup> G. Caglioti, E. De Agostino, F. Marsili, A. Paoletti, U. Pellegrini, and F. P. Ricci, *Nuovo Cimento Suppl.* **23**, 17 (1962).

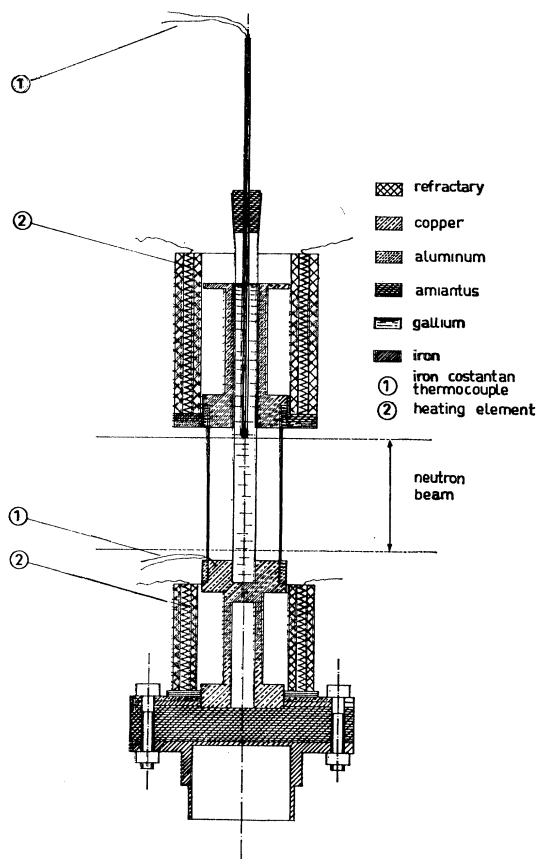


FIG. 1. The sample holder.

the capillary tube, which was dipped into the liquid gallium so as to skim the irradiated region.

As a sensing element for an electronic control unit another iron-constantan thermocouple was used, the hot joint of which was directly soldered to the lower piece of copper. With this experimental setup (Fig. 1) it was possible to have a temperature gradient of about  $2^\circ$ , along the 5 cm of the irradiated sample, also for the higher temperature at which the experiment was performed.

The fluctuations registered by the measuring thermocouple were of about one degree.

The incident beam of monochromatic neutrons was monitored with a fission counter, and the number of scattered neutrons was counted with a  $B^{10}F_3$  detector for a pre-set number of monitor counts. The intensity at any scattering angle was measured stepwise every  $1^\circ$  of arc in the range  $3^\circ 14'$  to  $94^\circ 14'$ .

### 1.3 EXPERIMENTAL RESULTS

Figure 2 shows the intensity curves observed for liquid gallium at 50 and  $150^\circ\text{C}$ . These patterns have been corrected for the background, which has been calculated on the basis of measurements performed with the quartz container, when empty and when filled with

$B_4C$ , furthermore taking into account the transmission through liquid gallium.

This transmission has been measured, and a value has been found in good agreement with that of the BNL-325 compilation. In each pattern the data begin at approximately  $s = (4\pi/\lambda) \sin(\frac{1}{2}\varphi) = 0.4 \text{ \AA}^{-1}$ ; from this point the curve has arbitrarily been extrapolated to the  $s=0$  value.

Having taken into account the small-angle scattering due to compressibility of the liquid, the extrapolated intensity for  $s=0$  gives the measurement of both multiple and incoherent scattering.

The positions of the intensity peaks, compared with those obtained by other workers, are given in Table I. The position of the main peak does not seem to vary appreciably with temperature, but its intensity decreases with increasing temperature. The subsidiary maximum to the right of the main peak becomes less noticeable at higher temperatures owing to the broadening of the main peak.

### 1.4 ANALYSIS OF THE DIFFRACTION PATTERNS

The experimental patterns have been analyzed in order to determine the atomic radial distributions. The equation used is given by the well-known formula<sup>14</sup>

$$4\pi r^2 \rho(r) = 4\pi r^2 \rho_0 + \frac{2r}{\pi} \int_0^\infty si(s) \sin(rs) ds, \quad (1)$$

where  $\rho(r)$  is the density of atoms at distance  $r$  from the atom in the origin,  $\rho_0$  is the mean atomic density, and

$$i(s) = (I(s) - I(\infty)) / (I(\infty) - I_0). \quad (2)$$

In Eq. (2),  $I(s)$  is the observed neutron intensity corrected for the background, as previously described.  $I_0$  is the value of the extrapolated intensity for  $s=0$ , which is connected with scattering processes (multiple, incoherent, and coherent due to compressibility) that are isotropic to a very good approximation.  $I(\infty) = \lim_{s \rightarrow \infty} I(s)$  is defined as the constant intensity at large angles, where interference effects can no longer be observed.

As is shown in Eq. (1), a Fourier integral has to be performed in the range  $s=0$  to  $\infty$ , but in practice available experimental data are limited to a finite upper value  $s_{\text{max}}$  and to a lower value  $s_1$  of  $s$ .

As far as the upper value  $s_{\text{max}}$  is concerned, the  $\int_0^\infty$  has been replaced by  $\int_0^{s_{\text{max}}}$  in the calculation of Eq. (1), supposing  $I(s)$  equal to  $I(\infty)$  for  $s = s_{\text{max}}$ . The consequence of this hypothesis (the well-known termination error),<sup>15-17</sup> (see later) is the introduction of ghost ripples in the atomic radial distribution.

<sup>14</sup> N. S. Gingrich, Rev. Mod. Phys. 15, 90 (1943).

<sup>15</sup> J. Waser and V. Shomaker, Rev. Mod. Phys. 25, 671 (1953).

<sup>16</sup> C. J. Pings and H. H. Pallman, Rev. Mod. Phys. 35, 389 (1963).

<sup>17</sup> K. Furakawa, Rept. Progr. Phys. 25, 395 (1962).

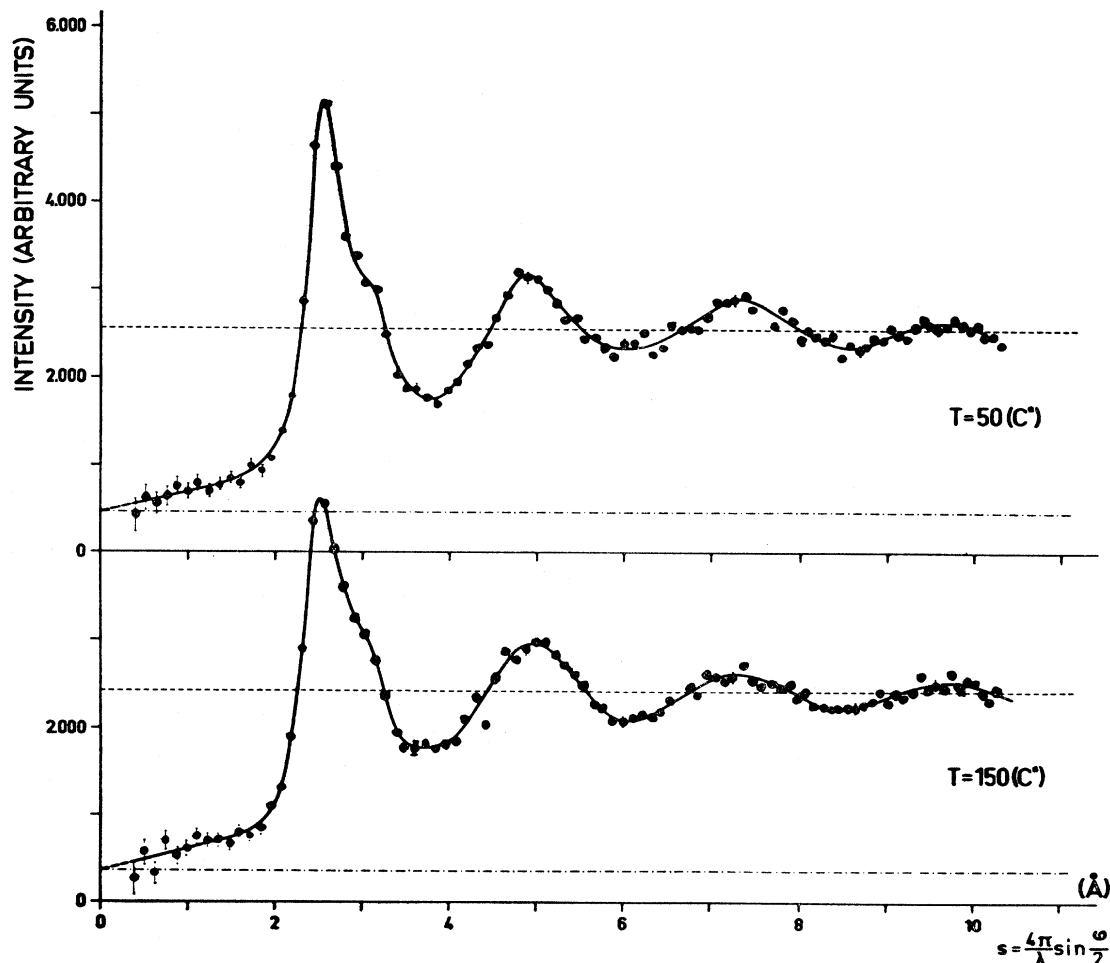


FIG. 2. Angular distribution of neutrons ( $\lambda=0.905 \text{ \AA}$ ) scattered by liquid gallium.

The value  $I(\infty)$  has been chosen to satisfy the relation

$$-2\pi^2\rho_0 = \int_0^{s_{\max}} s^2 i(s) ds. \quad (3)$$

The value of  $I(\infty)$  obtained in this way for the two diffraction patterns is indicated in Fig. 2, by a dotted line.

As far as the lower value  $s_1$  of  $s$  is concerned the intensity  $I(0)$  has been smoothly extrapolated to the value  $I_0$  at  $s=0$ .

Some remarks which must be made concerning this  $I_0$  level are given below, and the matter will be taken up again when the interatomic potential is considered (Sec. 3). The first point is that  $I_0$ , for experimental reasons, is established with a degree of uncertainty, of about 10% in our case. This uncertainty is reflected at most by an uncertainty of approximately 1% affecting the  $i(s)$  function [see Eq. (2)]. This uncertainty is nearly as great as that due to the experimental statistical errors (see Fig. 2), and other researchers have established that a reasonable possible

change in  $I_0$  level may give rise to alterations, which are not severe, in the resulting curves for atomic radial distributions.<sup>18</sup>

The second consideration is connected with the coherent small-angle scattering due to isothermal compressibility. If

$$\lim_{s \rightarrow 0} I(s) = I_0 \quad (4)$$

is accepted, from Eq. (2) we have

$$\lim_{s \rightarrow 0} i(s) = -1, \quad (5)$$

that is, the isothermal compressibility of the liquid is taken as zero. In fact, it is known (see Green,<sup>19</sup> p. 64) that in the region far from the critical point the following equality is obtained:

$$1 + i(0) = 1 + \int_0^\infty [\rho(r) - \rho_0] 4\pi r^2 dr = 10^{24} \times \chi_T \rho_0 K T, \quad (6)$$

<sup>18</sup> G. T. Clayton and L. Heaton, Phys. Rev. **121**, 649 (1961).

<sup>19</sup> H. Green, *Molecular Theory of Liquids* (North-Holland Publishing Company, Amsterdam, 1952).

TABLE I. Intensity patterns for liquid gallium.

Reference	Temp. (C°)	Peak position $s = (4\pi/\lambda) \sin(\varphi/2) [\text{Å}^{-1}]$				
		I	s.m.	II	III	IV
This work (neutron diffraction)	50	2.54±0.02	3.1±0.01	4.88±0.05	7.34±0.05	9.7 ±0.05
	150	2.52±0.02	3.1±0.01	4.96±0.05	7.34±0.05	9.74±0.05
Menke (Ref. 8) (x-ray diffraction)	18 undercooled	2.45	3.1	4.66	7.17	9.66
	45	2.45		4.66	7.17	9.66
Hendus (Ref. 9) (x-ray diffraction)	20 undercooled	2.5	2.83 <s.m.< 3.13	4.87	7.34	...

where  $\chi_T$  is the isothermal compressibility,  $\rho_0$  is the mean atomic density of the liquid (atoms/Å<sup>3</sup>),  $K$  is the Boltzmann constant, and  $T$  is the temperature.

For liquid gallium  $10^{24} \rho_0 K T \chi_T$  is equal to  $10^{-2}$  or  $0.6 \times 10^{-2}$ , depending on the value one selects for  $\chi_T$  ( $\chi_T = 4 \times 10^{-12}$ <sup>20</sup> or  $2.3 \times 10^{-12}$ <sup>21</sup> respectively).

This small-angle coherent scattering can be neglected as far as our interest in atomic radial distribution functions (far from critical point) is concerned. This is mainly due to the following circumstances:

(a) When  $s$  is small  $si(s)$  is small also,<sup>17</sup> and the contribution to the integral in (1) deriving from the lower  $s$  region is slight.

(b) The value of the integral  $\int_0^\infty [\rho(r) - \rho_0] 4\pi r^2 dr$  would eventually vary by about 1% from -1, and this variation is, at this stage, quite negligible.

## SECTION 2

### 2.1 ATOMIC RADIAL DISTRIBUTION FUNCTIONS AND ERRORS

Figure 3 shows the radial distribution functions for liquid gallium at 50 and 150°C. The positions and areas under the first peak are compared with those obtained by other workers in Table II.

Although it is not yet well defined how the area under the first peak is designated, in the present work the areas have been calculated by four methods (Figs. 4, 5).

(a) The right-hand side of the first peak area is made symmetrical with that on the left. The number of atoms calculated by this method may evidently be considered as a lower limit, but in fact no reliable physical reason supports the minimizing of the contribution from atoms in other coordination shells.

(b) The area is given by

$$\int_{r_1}^{r_2} 4\pi r^2 \rho(r) dr,$$

where  $r_1$  and  $r_2$  define the limits of the first peak. Although this method is considered the best mathematically, in many cases, when ripples affect the right part

of the first maximum (as in our case), its validity is, unfortunately, doubtful.

(c) The area is taken as that under the first peak, when the right-hand side of the peak is extrapolated to the abscissa. This is the most widely known method used, and is (in spite of the arbitrariness of the extrapolation) a reliable compromise among the other methods by which the first peak area may be evaluated.

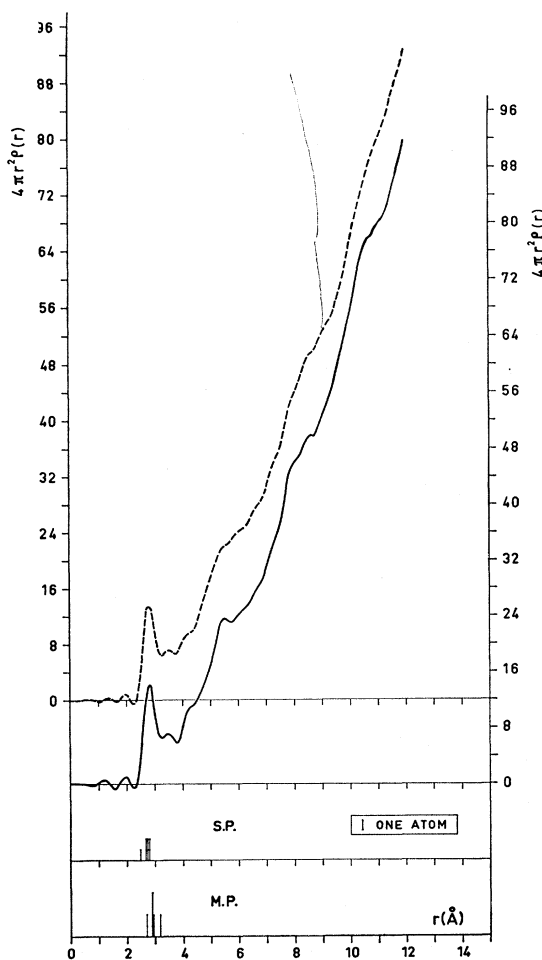


FIG. 3. Atomic radial distribution (a.r.d.) functions of liquid gallium. The full curve indicates the a.r.d. at  $T = 50^\circ\text{C}$ ; the dotted curve, at  $T = 150^\circ\text{C}$  (S.P. = stable phase; M.P. = metastable phase).

<sup>20</sup> P. Pascal, *Nouveau traité de Chimie Minérale* (Masson et Cie., Editeurs, Paris, 1961), p. 691.

<sup>21</sup> O. J. Kleppa, *J. Chem. Phys.* **18**, 1331 (1950).

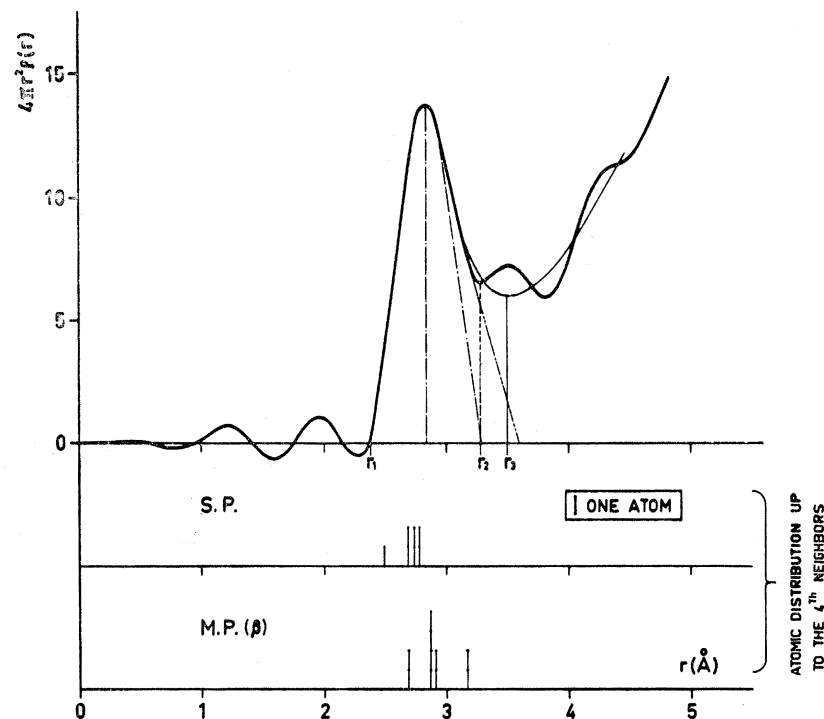


FIG. 4. Possible ways to calculate the area of the first peak in the atomic radial distribution of liquid gallium at  $T=50^{\circ}\text{C}$ : (i). The right-hand side of the first peak is made symmetrical with that on the left. (ii). The area is calculated by the integral  $\int_{r_1}^{r_2} 4\pi r^2 \rho(r) dr$ , where  $r_1$  and  $r_2$  define the limits of the first peak. (iii). The area is taken as that under the first peak, when the right-hand side of the peak is extrapolated to the abscissa. (iv). The area is calculated by the integral  $\int_{r_1}^{r_3} 4\pi r^2 \rho(r) dr$ , where  $r_1$  and  $r_3$  define the limits of the first peak and when the ripples, which affect the right-hand part of the first maximum, having been considered as caused by the termination error, have been arbitrarily suppressed.

(d) The area is calculated by

$$\int_{r_1}^{r_3} 4\pi r^2 \rho(r) dr,$$

where  $r_1$  and  $r_3$  define the limits of the first peak and when the ripples which affect the right part of the first maximum, having been considered as caused by the termination error, have been arbitrarily suppressed. A smooth idealized mean  $4\pi r^2 \rho(r)$  curve (light line in Figs. 4 and 5) has been drawn in this region. In any case it is reasonable to assume that the true number of atoms connected with the first peak area is contained

between the values calculated with methods (c) and (d), i.e.,  $9 \leq n \leq 9.6$  for  $T=50^{\circ}\text{C}$  and  $8.4 \leq n \leq 9.1$  for  $T=150^{\circ}\text{C}$ . In Table III the positions of the first peak in the radial atomic distributions together with the number of atoms in the first shell for the temperatures  $T=50$  and  $150^{\circ}\text{C}$  are compared with the positions and numbers of surrounding atoms, up to the fourth-nearest neighbors of the stable solid phase and the metastable phase  $\beta$ . Although the structure of the metastable phase  $\gamma$  has not yet been determined exactly because of experimental difficulties, very recently its density<sup>4</sup> has been measured, and it is reported in Table III. The density of this phase is slightly lower than that

TABLE II. Atomic radial distribution functions (R.D.F.) for liquid gallium.

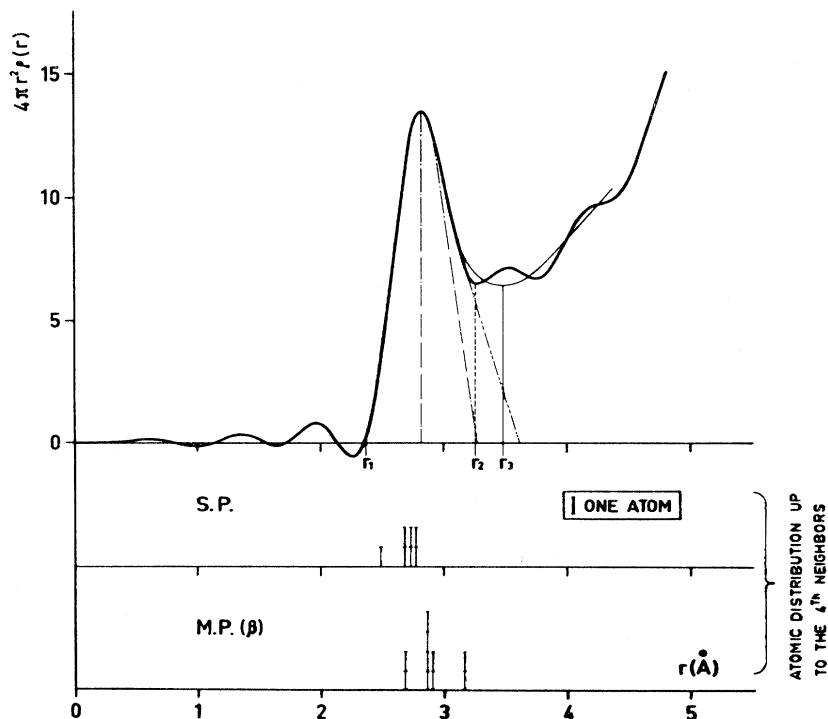
Reference	Temp. ( $^{\circ}\text{C}$ )	Position of first peak ( $\text{\AA}$ )	Peak made symmetrical	Area under first peak (number of atoms)						
				$\int_{r_1}^{r_2} 4\pi r^2 \rho(r) dr$			With spurious ripple suppressed			R.D.F. extrapolated to abscissa
				$r_1$	$r_2$		$r_1$	$r_2$		
This work (neutrons) $s_{\text{max}} = 10.24 \text{ \AA}^{-1}$	50	$2.84 \pm 0.02$	7.2	8.07	2.38	3.28	9.63	2.38	3.5	9
	150	$2.82 \pm 0.02$	6.78	7.63	3.37	3.26	9.1	2.37	3.48	8.35
This work $s_{\text{max}} = 6.6 \text{ \AA}^{-1}$	50	$2.9 \pm 0.05$	9.3	9.87	2.2	3.6				10
	Menke <sup>a</sup> (x rays)	18 45	2.83							Reported by Hendus 14-15
Hendus <sup>b</sup> (x rays)	20	2.77								11
H. Richter and S. Steeb <sup>c</sup> (electrons)	room temperature	2.79								9

<sup>a</sup> Reference 8.

<sup>b</sup> Reference 9.

<sup>c</sup> Reference 10.

FIG. 5. Possible ways to calculate the area of the first peak in the atomic radial distribution of liquid gallium at  $T=150^\circ\text{C}$ : (i). The right-hand side of the first peak is made symmetrical with that on the left. (ii). The area is calculated by the integral  $\int_{r_1}^{r_2} 4\pi r^2 \rho(r) dr$ , where  $r_1$  and  $r_2$  define the limits of the first peak. (iii). The area is taken as that under the first peak, when the right-hand side of the peak is extrapolated to the abscissa. (iv). The area is calculated by the integral  $\int_{r_1}^{r_3} 4\pi r^2 \rho(r) dr$ , where  $r_1$  and  $r_3$  define the limits of the first peak and when the ripples, which affect the right-hand part of the first maximum, having been considered as caused by the termination error, have been arbitrarily suppressed.



of the  $\beta$  phase but always higher than that of the liquid phase, undercooled at a temperature of  $-35.6^\circ\text{C}$ .

The errors on the atomic radial distribution functions have been considered along the lines of Refs. 15 and 16.

As was suggested in Ref. 15 the termination error has been studied on the function  $4\pi r \rho(r)$  rather than on  $4\pi r^2 \rho(r)$ . This has been done in order to study the direct result of the Fourier transform (apart from an additive factor  $4\pi r \rho_0$ ) [see Eq. (1)]; in fact, the conventional multiplication of  $4\pi r \rho(r)$  by  $r$  introduces a certain amount of asymmetry and shift into the aberrations, which might affect the real unknown curve.

The spurious features introduced by truncating the formal infinite Fourier integral [Eq. (1)] at a value  $s=s_{\text{max}}$  display themselves approximately as: (i) "ghost" ripples on either side of the first main peak in

$4\pi r \rho(r)$ , showing maxima at distances<sup>17</sup>

$$\Delta r \approx \frac{5\pi}{2s_{\text{max}}}, \frac{9\pi}{2s_{\text{max}}}, \dots$$

from the position of the main peak; and (ii) broadening of the main peak.

$\Delta r$  has been calculated for  $s_{\text{max}}=10.24 \text{ \AA}^{-1}$  and also for  $s_{\text{max}}=6.6 \text{ \AA}^{-1}$ . The calculated values, which should be temperature-independent, are compared with the experimental results in Table IV.

The good agreement (see Table IV) between the observed and calculated values of the position of the "ghost" maxima indicates that the radial distribution functions are clearly influenced by the termination error.

TABLE III. Comparison of liquid and solid phases of gallium.

	Liquid gallium	Solid gallium metastable phase ( $\text{Ga}\gamma$ ) <sup>a</sup>	Solid gallium metastable phase ( $\text{Ga}\beta$ ) <sup>b</sup>	Solid gallium stable phase ( $\text{GaI}$ ) <sup>c</sup>
Melting point		$-35.6^\circ\text{C}$	$-16.3^\circ\text{C}$	$+29.78^\circ\text{C}$
Density (g/cc)	6.153 at $-35.6^\circ\text{C}$ 6.136 at $-16.3^\circ\text{C}$ 6.09 at $+29.80^\circ\text{C}$	6.20 This metastable phase is more compact than the liquid	6.23 This metastable phase is more compact than the liquid	The stable phase less compact than the liquid 5.90 at $29.65^\circ\text{C}$
Neighboring atoms	9-9.5 atoms at $2.84 \pm 0.02 \text{ \AA}$ at $T=50^\circ\text{C}$		2 atoms at $2.68 \text{ \AA}$ 4 atoms at $2.87 \text{ \AA}$ 2 atoms at $2.90 \text{ \AA}$ 2 atoms at $3.17 \text{ \AA}$	1 atom at $2.44 \text{ \AA}$ 2 atoms at $2.70 \text{ \AA}$ 2 atoms at $2.74 \text{ \AA}$ 2 atoms at $2.795 \text{ \AA}$

<sup>a</sup> See Ref. 29.

<sup>b</sup> See Ref. 11. The gallium atoms are grouped in zig-zag chains. The distances between two atoms in the chain is  $2.68 \text{ \AA}$  and the angle Ga-Ga-Ga is  $72^\circ 30'$ .

<sup>c</sup> See Ref. 20. Each atom has one neighbor very near. The possible existence of a  $\text{Ga}_2$  molecule has been suggested.

TABLE IV. Ghost ripples in the radial distributions functions due to the termination effect.

	Left-hand side of main peak		Right-hand side of main peak	
	Position of first ripple ( $\text{\AA}$ )	Position of second ripple ( $\text{\AA}$ )	Position of first ripple ( $\text{\AA}$ )	Position of second ripple ( $\text{\AA}$ )
Observed $T=50^\circ\text{C}$ , $s_{\text{max}}=10.24 \text{ \AA}^{-1}$	$1.25 \pm 0.05$	$1.95 \pm 0.03$	$3.48 \pm 0.03$	$4.3 \pm 0.05$
Observed $T=150^\circ\text{C}$ , $s_{\text{max}}=10.24 \text{ \AA}^{-1}$		$1.98 \pm 0.03$	$3.46 \pm 0.03$	$4.16 \pm 0.05$
Calculated $\left( \pm \frac{5\pi}{2s_{\text{max}}}; -\frac{9\pi}{2s_{\text{max}}}; \dots \right)$	$1.43 \pm 0.02$	$2.05 \pm 0.02$	$3.48 \pm 0.02$	$4.20 \pm 0.02$
Observed $T=50^\circ\text{C}$ , $s_{\text{max}}=6.6 \text{ \AA}^{-1}$	$0.74 \pm 0.05$	$1.59 \pm 0.03$	vanishing	
Calculated $\left( \pm \frac{5\pi}{2s_{\text{max}}}; -\frac{9\pi}{2s_{\text{max}}}; \dots \right)$	$0.74 \pm 0.02$	$1.69 \pm 0.02$	$4.07 \pm 0.02$	

In Fig. 6 the  $4\pi r^2\rho(r)$  curves are shown for  $s_{\text{max}}=10.24 \text{ \AA}^{-1}$  and  $s_{\text{max}}=6.6 \text{ \AA}^{-1}$ , respectively.

The position and the area under the first peak in the radial distribution function connected with the value of  $s_{\text{max}}=6.6 \text{ \AA}^{-1}$  ( $T=50^\circ$ ) are compared with those corresponding to  $s_{\text{max}}=10.24 \text{ \AA}^{-1}$  in Table II.

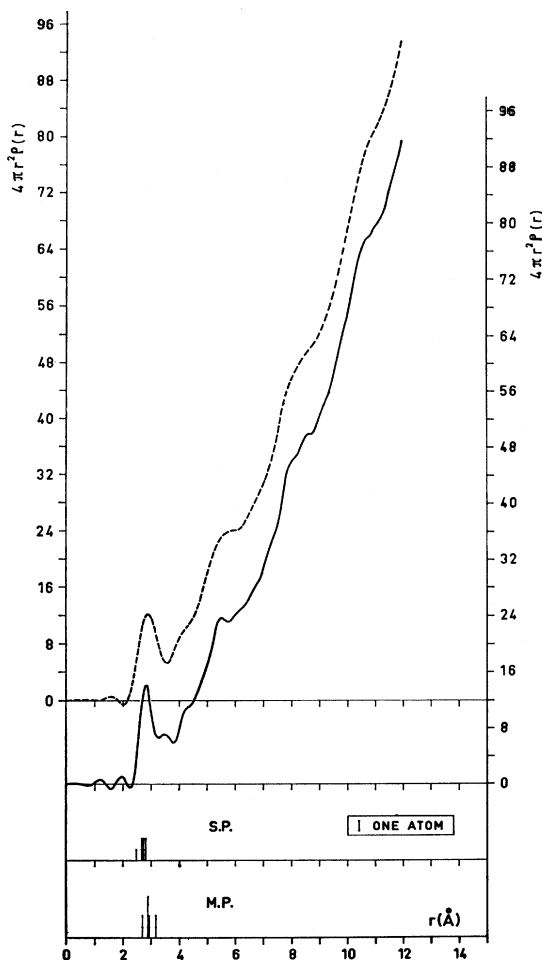


FIG. 6. Atomic radial distribution function of liquid gallium. The full curve indicates the a.r.d. calculated by data terminated at  $s_{\text{max}}=10.24 \text{ \AA}^{-1}$ , at  $T=50^\circ\text{C}$ ; the dotted curve, at  $s_{\text{max}}=6.6 \text{ \AA}^{-1}$ ,  $T=50^\circ\text{C}$ .

A rough evaluation of the broadening of the main peak induced by the termination error can be made if a Gaussian approximation is accepted. That is, the real unknown main peak in  $4\pi r^2\rho(r)$  and the modification function folding with it are taken to be approximately of the Gaussian type. On this basis, as far as the width at half-maximum of the main peak is concerned, one can say that the two curves for  $T=50$  and  $T=150^\circ\text{C}$  are broadened less than 10% by the modifying function. Unfortunately, this evaluation does not give any information about the eventual variation of the area of the first peak in the  $4\pi r^2\rho(r)$  distribution, because it is well known that, when the range 0 to  $s_{\text{max}}$  of the Fourier integration is increased, this peak becomes more and more squeezed and sharper in a rather unexpected way. For comparison see the discussion on this area in Refs. 18 and 22.

### SECTION 3

#### 3.1 THE INTERATOMIC POTENTIAL FROM NEUTRON-DIFFRACTION PATTERNS

Some years ago Percus and Yevick presented one of the most promising among the approximate theories of fluids,<sup>12</sup> by which the atomic radial distribution can be deduced directly from the interatomic forces, which are assumed pairwise and central.

It is not the purpose of this work to test the validity of this theory, which is widely discussed elsewhere,<sup>23-25</sup> but only to use its final result in order to derive a force law between atoms in a liquid once the neutron-diffraction pattern is known.

Let us recall the final form of the (PY) integral equation

$$e^{\phi(r)/KT}[\rho(r)/\rho_0] = 1 - \rho_0 \int \left[ (e^{\phi(l)/KT} - 1) \frac{\rho(l)}{\rho_0} \right] \left[ \frac{\rho(r-l)}{\rho_0} - 1 \right] dl, \quad (7)$$

<sup>22</sup> G. Caglioti and F. P. Ricci, Nuovo Cimento 24, 103 (1962).

<sup>23</sup> A. A. Broyles, S. U. Chung, and H. L. Sahlén, J. Chem. Phys. 37, 2462 (1962).

<sup>24</sup> A. A. Khan, Phys. Rev. 134, A367 (1964).

<sup>25</sup> A. A. Khan, Phys. Rev. 136, A1260 (1964).

where  $\rho(\mathbf{r})/\rho_0$  is the two-body distribution function,  $\rho_0$  the mean atomic density,  $\phi(\mathbf{r})$  the mutual potential energy of a pair of atoms separated by a distance  $r$ ,  $K$  the Boltzmann constant, and  $T$  the temperature in degrees Kelvin.

The equation is then written in the following form:

$$(e^{\phi(\mathbf{r})/KT} - 1)\rho(\mathbf{r}) + \rho(\mathbf{r}) - \rho_0 = - \int [(e^{\phi(\mathbf{l})/KT} - 1)\rho(\mathbf{l})][\rho(\mathbf{r}-\mathbf{l}) - \rho_0] d\mathbf{l}. \quad (8)$$

Let us introduce the two Fourier transforms:

$$f(\mathbf{s}) = \int [(e^{\phi(\mathbf{r})/KT} - 1)\rho(\mathbf{r})] e^{i\mathbf{s}\cdot\mathbf{r}} d\mathbf{r}, \quad (9)$$

$$i(\mathbf{s}) = \int [\rho(\mathbf{r}) - \rho_0] e^{i\mathbf{s}\cdot\mathbf{r}} d\mathbf{r}. \quad (10)$$

If we multiply each member of Eq. (8) by  $e^{i\mathbf{s}\cdot\mathbf{r}} d\mathbf{r}$  and perform the integration on  $\mathbf{r}$ , Eq. (8) is reduced to the simple expression

$$f(\mathbf{s}) + i(\mathbf{s}) = -i(\mathbf{s})f(\mathbf{s}) \quad (11)$$

or

$$f(\mathbf{s}) = -i(\mathbf{s})/[i(\mathbf{s}) + 1]. \quad (12)$$

Considering  $\rho(\mathbf{r})$  and  $\phi(\mathbf{r})$  independent of the solid angle and integrating the exponential function  $e^{i\mathbf{s}\cdot\mathbf{r}}$  over it, the following relations are deduced:

$$f(s) = \int_0^\infty (e^{\phi(r)/KT} - 1)\rho(r) \frac{\sin(rs)}{rs} 4\pi r^2 dr, \quad (9')$$

$$i(s) = \int_0^\infty [\rho(r) - \rho_0] \frac{\sin(rs)}{rs} 4\pi r^2 dr, \quad (10')$$

or, by Fourier inversion,

$$4\pi r^2 (e^{\phi(r)/KT} - 1)\rho(r) = \frac{2r}{\pi} \int_0^\infty s f(s) \sin(rs) ds, \quad (9'')$$

$$4\pi r^2 \rho(r) = 4\pi r^2 \rho_0 + \frac{2r}{\pi} \int_0^\infty s i(s) \sin(rs) ds. \quad (10'')$$

It is noted that Eq. (10'') is exactly expression (1) of this paper, the notations having the same meaning. By eliminating the quantity  $4\pi r^2 \rho(r)$  by the Eqs. (9'') and (10'') we now obtain

$$e^{\phi(r)/KT} - 1 = \frac{(2r/\pi) \int_0^\infty s f(s) \sin(rs) ds}{4\pi r^2 \rho_0 + (2r/\pi) \int_0^\infty s i(s) \sin(rs) ds}. \quad (13)$$

If we recall the expression for  $f(\mathbf{s})$  in Eq. (12), we finally obtain:

$$\phi(r) = KT \ln \left[ 1 - \frac{(2r/\pi) \int_0^\infty s \{i(s)/[i(s)+1]\} \sin(rs) ds}{4\pi r^2 \rho_0 + (2r/\pi) \int_0^\infty s i(s) \sin(rs) ds} \right]. \quad (14)$$

This formula permits us to derive directly the mutual potential energy  $\phi(r)$  between pairs of atoms once the  $i(s)$  function defined in terms of the neutron diffraction patterns in expression (2) of this paper is known. Relation (14) has been used in order to find the mutual potential between pairs of atoms in liquid gallium. Owing to the fact that gallium is a metal, and following the recent theories of electronic properties of liquid metals, it can be argued that this potential may give a fair description of the ion-ion interaction in liquid gallium. Equivalent forms of Eq. (14) can be easily derived from it. The final results are reported here, their derivation being described in the Appendix:

$$\phi(r) = U(r) + KT \ln \left[ 1 + \frac{1}{2\pi^2 r \rho_0} \times \int_0^\infty \frac{s i(s)^2}{i(s)+1} \sin(rs) ds \right], \quad (14')$$

$$\phi(r) = U(r) + KT \ln \left\{ 1 - \frac{2\pi}{r \rho_0} \int_0^\infty (e^{\phi(y)/KT} - 1) \rho(y) y dy \times \int_{r-y}^{r+y} r [\rho(r) - \rho_0] dr \right\}, \quad (14'')$$

where  $U(r)$  is defined in the usual way (see Green,<sup>19</sup> p. 75) as

$$\rho(r)/\rho_0 = e^{-[U(r)/KT]}, \quad (15)$$

and has the meaning of a mean potential energy of a pair of atoms in the configuration  $\rho(r)/\rho_0$ .

### 3.2 INACCURACIES IN THE FOURIER TRANSFORM OF THE FUNCTION $f(s)$

In order to find the ion-ion potential by formula (14), two Fourier integrals have to be calculated. One of them,  $\int_0^\infty s i(s) \sin(rs) ds$ , has been discussed in Sec. 1.4; here we are interested in the second one; that is,

$$F_1(r) = (2r/\pi) \int_0^\infty \frac{i(s)}{i(s)+1} \sin(rs) ds. \quad (16)$$

The consequences of limiting the range of integration (0 to  $s_{\max}$ ) have been studied in the same way as in Eq. (2) and in general, we have nothing to add to what has already been said. Nevertheless, we should stress that the termination error influences  $F_1(r)$  at small and medium  $r$  but not at large  $r$ . This is important because it can be concluded that the termination error does not affect the long-range behavior of the potential  $\phi(r)$  [see Fig. (7)]. Major attention has to be paid to the effect of  $i(s)/i(s)+1$  for  $s \rightarrow 0$  on  $F_1(r)$ .

Remembering (12) and (9), we derive

$$\frac{i(s)}{i(s)+1} = - \int_0^\infty (e^{\phi(r)/KT} - 1) \rho(r) \frac{\sin(rs)}{rs} 4\pi r^2 dr. \quad (17)$$

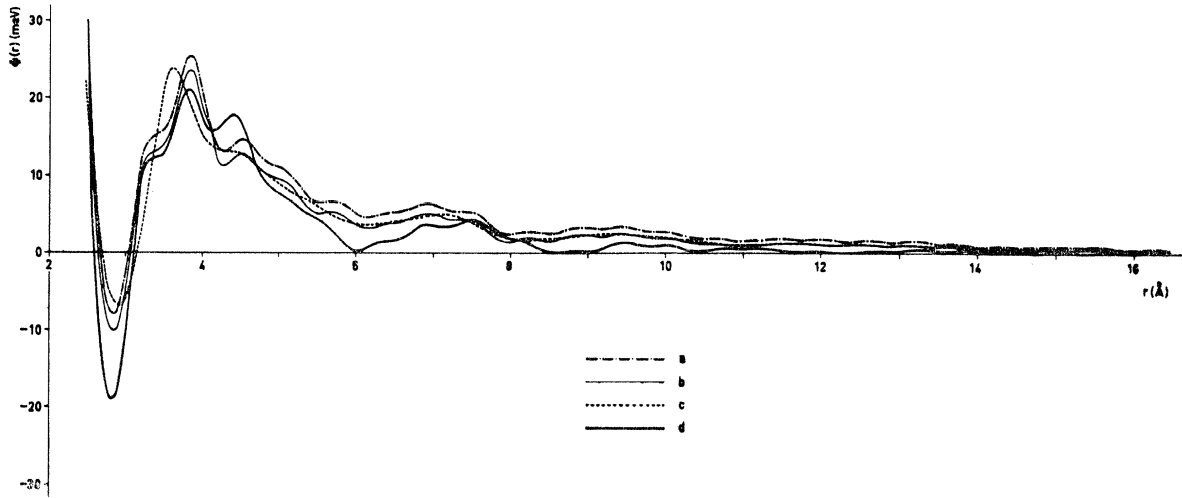


Fig. 7. Ion-ion potential in liquid gallium. The curves a, b, c, d refer to the following values of the temperature  $T$  and isothermal compressibility  $\chi_T$ : (a)  $T=50^\circ\text{C}$ ;  $\chi_T=2.4\times 10^{-12}$  cm<sup>2</sup>/dyn; (b)  $T=50^\circ\text{C}$ ;  $\chi_T=4\times 10^{-12}$  cm<sup>2</sup>/dyn; (c)  $T=50^\circ\text{C}$ ;  $\chi_T=4\times 10^{-12}$  cm<sup>2</sup>/dyn, the intensity data used having been arbitrarily terminated at  $s_{\text{max}}=6.6$  Å<sup>-1</sup>; (d)  $T=150^\circ\text{C}$ ;  $\chi_T=4.5\times 10^{-12}$  cm<sup>2</sup>/dyn.

This means that

$$\frac{i(0)}{i(0)+1} = - \int_0^\infty (e^{\phi(r)/KT} - 1) \rho(r) 4\pi r^2 dr. \quad (18)$$

It is clearly impossible to take the approximate value  $(-1)$  for  $i(0)$ ; in fact, in this case, the integral in (17) would diverge, which is not acceptable because

$$\lim_{r \rightarrow \infty} \phi(r) = 0$$

and

$$\lim_{r \rightarrow \infty} \rho(r) = \rho_0.$$

(See Green.<sup>19</sup>)

For this reason, we have taken into account the small-angle scattering contribution due to isothermal compressibility. Besides, from (6) we find

$$\frac{1 - 10^{24} \chi_T \rho_0 K T}{10^{24} \chi_T \rho_0 K T} = + \int_0^\infty (e^{\phi(r)/KT} - 1) \rho(r) \times 4\pi r^2 dr. \quad (19)$$

Observing (19) we see that the situation here is clearly different from that discussed in Sec. 1.4(a), the integral in (19) being extremely sensitive to the value of  $i(0)$  or in particular to the isothermal compressibility (IC) (see also Khan, Ref. 25).

A rough argument can be given to confirm this conclusion (for liquids far from critical point), if notice is taken of the fact that, comparing (6) and (19) for a given range of  $\chi_T - s$ , we find

$$0 \leq \chi_T \simeq \chi_T^* \simeq 4 \times 10^{-12} \text{ cm}^2/\text{dyn},$$

$$-1 \leq \int_0^\infty [\rho(r) - \rho_0] 4\pi r^2 dr \leq -0.98$$

$$0 \leq \chi_T \leq \chi_T^* \simeq 4 \times 10^{-12} \text{ cm}^2/\text{dyn},$$

$$\infty \geq \int_0^\infty (e^{\phi(r)/KT} - 1) \rho(r) 4\pi r^2 dr \geq 10^2.$$

The numerical value of  $\chi_T^*$  should be considered as an order of magnitude of the IC. (In particular, we have chosen the IC of gallium reported in Ref. 20.)

The argument given above suggests the need for independent exact determination of the IC in liquids, as well as for accurate neutron-diffraction intensity measurements for small scattering angles. However, as far as the IC is concerned, we should point out that unfortunately the (PY) theory does not give good results. Nevertheless, in order to see the effects of a small change in the IC both  $F_1(r)$  and  $\phi(r)$  have been found for two different values of  $\chi_T$  (see Fig. 7).

### 3.3 ION-ION POTENTIAL IN LIQUID GALLIUM

By expression (14) the ion-ion potential in liquid gallium has been derived in particular:

(a) From the observed intensity data on gallium at  $50^\circ\text{C}$ , using a value of the isothermal compressibility  $\chi_i = 2.4 \times 10^{-12}$  cm<sup>2</sup>/dyn from Ref. 21.

(b) From the observed intensity data on gallium at  $50^\circ\text{C}$ , using a value of the isothermal compressibility  $\chi_i = 4 \times 10^{-12}$  cm<sup>2</sup>/dyn from Ref. 20, which is almost the same as that of mercury at  $50^\circ\text{C}$ .

(c) From the observed intensity data on gallium at  $50^\circ\text{C}$ , arbitrarily terminated at  $s_{\text{max}} = 6.6$  Å<sup>-1</sup>, and using a  $\chi_i = 4 \times 10^{-12}$  cm<sup>2</sup>/dyn.

(d) From the observed intensity data on gallium at  $150^\circ\text{C}$ , with a value of the isothermal compressibility  $\chi_i = 4.5 \times 10^{-12}$  cm<sup>2</sup>/dyn equal to that of mercury at  $150^\circ\text{C}$ , this because Ref. 21 gives  $\chi_i$  at  $50^\circ\text{C}$  only.

These different  $\phi(r)$  curves are shown in Fig. 7.

We observe, respectively, for case

(a') A minimum at  $r=2.85 \text{ \AA}$  with a depth of  $-8 \text{ meV}$ , a maximum at  $r=3.85 \text{ \AA}$  with a height of  $25 \text{ meV}$ .

(b') A minimum at  $r=2.85 \text{ \AA}$  with a depth of  $-10 \text{ meV}$ , a maximum at  $r=3.85 \text{ \AA}$  with a height of  $22.5 \text{ meV}$ .

(c') A minimum at  $r=2.9 \text{ \AA}$  with a depth of  $-7.5 \text{ meV}$ , a maximum at  $r=3.6 \text{ \AA}$  with a height of  $23.5 \text{ meV}$ .

(d') A minimum at  $r=2.85 \text{ \AA}$  with a depth of  $-19.5 \text{ meV}$ , a maximum at  $r=3.8 \text{ \AA}$  with a height of  $21 \text{ meV}$ , and for the long-range tail with defined oscillatory behavior, the positions of the minima are  $r \cong 6, 9, 12, \text{ and } 15 \text{ \AA}$  etc.

A comparison of the curves indicated as  $a$  and  $b$  shows that an error in the correct value of the isothermal compressibility roughly reflects itself as an uncertainty in the zero level of the energy scale; at least this is true for not too high values of  $r$ .

The effect produced by the termination error (see also Sec. 3.2), which can be appreciated by comparing curves  $b$  and  $c$  (Fig. 7) seems to influence mainly the short-range part of  $\phi(r)$ ; in fact the two curves coincide for  $r > 7 \text{ \AA}$ .

Moreover, we remark that the ripples appearing on each side of the first maximum in  $\phi(r)$  at about  $3.5$  and  $4.2 \text{ \AA}$  are clearly spurious [cf. analogous spurious ripples already discussed for  $4\pi r^2 \rho(r)$  in Fig. 6].

Long-range oscillatory interactions between ions in a liquid metal have been pointed out earlier by Johnson and March<sup>26</sup> and recently reported by Johnson *et al.*<sup>27</sup> These authors analyzed the atomic radial distributions functions for eight liquid metals.

The long-range form of the interaction is given by

$$\phi(r) = \cos(2K_f r) / r^3,$$

where  $K_f$  is the radius of the Fermi sphere, assuming that the screening is due to free electrons, with a Fermi momentum distribution.

This long-range oscillatory behavior is not found for the  $\phi(r)$  of gallium at  $T=50^\circ\text{C}$ . In contrast, an ill-defined oscillating feature can be identified in the  $\phi(r)$  for  $T=150^\circ\text{C}$ .

Moreover, the  $\phi(r)$  for  $T=150^\circ\text{C}$  displays a deeper minimum than the  $\phi(r)$  for  $T=50^\circ\text{C}$ . Let us now suggest one of the causes that could have generated these features. We shall try to justify them physically in the following section.

The "anomalies" could well arise from the rather arbitrary way of extrapolating the observed intensity to zero angle (see Fig. 2), especially for the intensity pattern for  $T=50^\circ\text{C}$ . Unfortunately, until now, no analytic small-angle asymptotic form of the structure factor (see Fig. 2) has been proposed for a liquid metal.<sup>28</sup>

<sup>26</sup> M. D. Johnson and N. H. March, Phys. Letters 3, 313 (1963).

<sup>27</sup> M. D. Johnson, P. Hutchinson, and N. H. March, Proc. Roy. Soc. (London) 282, A283 (1964).

<sup>28</sup> Recently, J. E. Enderby, T. Gaskell, and N. H. March, Proc. Phys. Soc. (London) 85, 217 (1965), discussed the asymptotic form of correlation functions in classical fluids and in liquid

## SECTION 4

### 4.1 DISCUSSION

It seems rather difficult to interpret the results we have obtained either for the structure or for the ion-ion potential of liquid gallium, inasmuch as data and conclusions on gallium electronic properties published so far are often conflicting. The values for electronic transport properties reported by Cusack *et al.*,<sup>7</sup> are in fact difficult to reconcile with the interpretation and the results of positron-annihilation measurements on solid and liquid gallium by Stewart *et al.*,<sup>5</sup> and by Gustafson and Mackintosh.<sup>6</sup> Nevertheless, by the position of the first coordination shell, by the number of atoms in this shell and by a comparison reported in Table III, we might argue that the structure of liquid gallium, at least at temperatures not far from the melting point and on a short-range order scale, displays the main features of the structure of the metastable solid  $\beta$  phase.

The exact structure of the metastable  $\gamma$  phase is not known, but in Ref. 29 it is reported that the smallest distance between two atoms is  $2.44 \text{ \AA}$ , as in the stable solid phase. This distance  $2.44 \text{ \AA}$  has not been resolved in the liquid structure. For this reason we exclude at the moment the idea that the liquid could have a structure similar to that of the  $\gamma$  phase.

The metastable  $\beta$  phase is stable at very high pressure,<sup>20</sup> while at room temperature and at normal pressure it has a density larger than the stable phase. This means that ions set in a situation such as that displayed by the structure of the  $\beta$  phase experience a strong repulsive field. We can say that the potential of curve  $a$ , Fig. 7 may be justified by a situation of "quasimetastability" of the liquid phase near the melting point, the ion experiencing a long-range repulsive potential with a small potential well at short range. When the temperature is raised, the density is lowered; the volume occupied by every ion increases and the configuration of the liquid evolves to a higher degree of stability, which is described by potential curve  $d$ .

The electrical resistivity  $\rho_\beta$  of the metastable phase has been measured.<sup>30</sup> The ratio  $K = \rho_L / \rho_\beta$  of the resistivity of liquid gallium to that of metastable  $\beta$  phase is in the range  $2.2 \leq K \leq 3$ . It is remarkable that a value of  $2.2 \leq K \leq 3$  connects gallium with the other elements of its group, as is reported in Table V, in a certain sense "renormalizing" the situation.

It is interesting to note that the Mott formula<sup>2,31</sup>

$$\rho_L / \rho_s = \exp(80L / T_m) \quad (L \text{ in } kJ/\text{mole}, T_m \text{ in } ^\circ\text{K}),$$

helium 4. In this paper they present an expansion for small  $s$  of the structure factor of a classical insulating liquid. The structure factor for small  $s$  of a liquid metal is not discussed.

<sup>29</sup> P. Blaconnier, thesis, Faculté des sciences de l'Université de Paris, 1964 (unpublished).

<sup>30</sup> L. Bosio, A. Defrain, and I. Elpboin, Compt. Rend. 250, 2553 (1960).

<sup>31</sup> N. Cusack and J. E. Enderby, Proc. Phys. Soc. (London) 75, 395 (1960).

TABLE V. Ratio of resistivities of liquid and solid phases for elements of the gallium group.

	Al	Ga ( $\beta$ )	In	Tl
$K$	2.2	$2.2 \leq K \leq 3$	2.18	2.06

connecting the ratio of the resistivity of the liquid and of the solid phase with the latent heat of fusion  $L$  and with the melting temperature  $T_m$ , gives a value of  $K=2.29$ , which is in agreement with the experimental one, when we take the value<sup>32</sup> 9.09 cal/g as the latent heat of fusion of the metastable  $L_\beta$  phase, at the melting temperature  $T_m = -16.3^\circ\text{C}$ .

Nevertheless, it is doubtful whether Mott's theory can apply to gallium, because  $\rho_L$  is not proportional to the absolute temperature, as one of the assumptions of this theory<sup>31</sup> requires.

Finally, recalling that we obtained  $9 \leq n \leq 9.6$  atoms in the first coordination shell for gallium at  $T=50^\circ$  and  $8.4 \leq n \leq 9.1$  for gallium at  $150^\circ\text{C}$ , it may be observed that a rough extrapolation predicts about  $n=7$  atoms for gallium in the range  $300 \lesssim T \lesssim 350$  and about  $n=10$  atoms for undercooled liquid gallium near the melting point ( $-16.3^\circ\text{C}$ ) of the  $\beta$  phase. This is in agreement at high temperature with the density of liquid gallium; this density at  $315^\circ\text{C}$ <sup>33</sup> being equal to that of the stable phase at the melting point  $29.7^\circ\text{C}$ ; and is in agreement at low temperature with the number of atoms in the first coordination shell for the  $\beta$  phase.

We think it would be very interesting to have confirmation of our hypothesis determining the structure of liquid undercooled gallium at a temperature near  $-16.3^\circ\text{C}$ .

## 4.2 CONCLUSIONS

The atomic radial distributions for liquid gallium at 50 and  $150^\circ\text{C}$  have been deduced by the observed neutron diffraction intensity patterns. An approximate form of the ion-ion interaction in liquid gallium at 50 and at  $150^\circ\text{C}$  has been obtained using the fundamental equation of the (PY) theory of liquid.

The (PY) equation has been set in a simple form suitable for the direct exploitation of neutron diffraction data. Equivalent forms of the (PY) equation have been derived. Analogies in the short-range structure of liquid gallium with the solid metastable  $\beta$  phase have been stressed. If the metastable  $\beta$  phase is considered as the parent solid phase of the liquid gallium, the melting behavior of gallium can be regarded as much more normal, at least as far as the changes in density and in electrical resistivity are concerned. The main features of the ion-ion interaction derived by the (PY) equation for liquid gallium seem to be justified if the analogy between liquid and solid metastable  $\beta$  phases is accepted.

## ACKNOWLEDGMENTS

It is a pleasure to thank Dr. N. Cusack (Department of Physics, Birkbeck College, London), and Professor N. H. March (Department of Physics, The University, Sheffield) for their encouraging comments on the manuscript. We are grateful to Professor G. Caglioti for the interest shown in this subject, to Professor M. H. Curien and Dr. A. Defrain of the Faculty of Sciences of the University of Paris for all the reprints and information they provided about the metastable phases of gallium. We are also indebted to Dr. J. Peretti of C. C. R. Euratom for discussions, to Dr. A. Cherubini for the Fourier transform programming, and to L. Esposito for vigorous technical assistance.

## APPENDIX

From Eq. (14) in the text we derive the following:

$$\phi(r) = KT \ln \left[ \frac{4\pi r^2 \rho(r) - (2r/\pi) \int_0^\infty s \{i(s)/[i(s)+1]\} \sin(rs) ds}{4\pi r^2 \rho(r)} \right].$$

Hence

$$\phi(r) = U(r) + KT \ln \left[ \frac{4\pi r^2 \rho_0 + (2r/\pi) \int_0^\infty s i(s) \sin(rs) ds - (2r/\pi) \int_0^\infty s \{i(s)/[i(s)+1]\} \sin(rs) ds}{4\pi r^2 \rho_0} \right],$$

having defined  $e^{-U(r)/KT} = \rho(r)/\rho_0$ .

Finally, by adding the two integrals in the above expression we obtain the Eq. (14') (see text):

$$\phi(r) = U(r) + KT \ln \left[ 1 + \frac{1}{2\pi^2 r \rho_0} \int_0^\infty s \frac{[i(s)]^2}{i(s)+1} \sin(rs) ds \right]. \quad (14')$$

<sup>32</sup> L. Bosio and A. Defrain, *Compt. Rend.* **258**, 4929 (1964).

<sup>33</sup> N. Cusack and P. Kendall, *Proc. Phys. Soc.* **75**, 309 (1960).

Rewriting the integral

$$\int_0^{\infty} s \frac{[i(s)]^2}{i(s)+1} \sin(rs) ds$$

in the form

$$\int_0^{\infty} s i(s) \frac{i(s)}{i(s)+1} \sin(rs) ds,$$

and recalling the definition of the function  $f(s)$  (see text), we obtain

$$\begin{aligned} -\int_0^{\infty} s f(s) i(s) \sin(rs) ds &= -\int_0^{\infty} \int_0^{\infty} (e^{\phi(y)/KT} - 1) \rho(y) \sin(ys) 4\pi y dy i(s) \sin(rs) ds \\ &= -\int_0^{\infty} (e^{\phi(y)/KT} - 1) \rho(y) 4\pi y dy \int_0^{\infty} i(s) \sin(ys) \sin(rs) ds \\ &= \int_0^{\infty} (e^{\phi(y)/KT} - 1) \rho(y) 4\pi y dy \left\{ \frac{1}{2} \int_0^{\infty} i(s) \cos[(r-y)s] ds - \frac{1}{2} \int_0^{\infty} i(s) \cos[(r+y)s] ds \right\}. \end{aligned}$$

Observing that

$$-\frac{d}{dr} \int_0^{\infty} i(s) \cos(rs) ds = + \int_0^{\infty} s i(s) \sin(rs) ds = 2\pi^2 r [\rho(r) - \rho_0],$$

we then derive

$$\int_0^{\infty} s \frac{[i(s)]^2}{i(s)+1} \sin(rs) ds = -4\pi^3 \int_0^{\infty} (e^{\phi(y)/KT} - 1) \rho(y) y dy \int_{r-y}^{r+y} r [\rho(r) - \rho_0] dr.$$

If we now substitute the above expression of the Fourier transform in Eq. (14'), we obtain Eq. (14'') (see text):

$$\phi(r) = U(r) + KT \ln \left\{ 1 - \frac{2\pi}{r\rho_0} \int_0^{\infty} (e^{\phi(y)/KT} - 1) \rho(y) y dy \int_{r-y}^{r+y} r [\rho(r) - \rho_0] dr \right\}. \quad (14'')$$

This equation has been used by Johnson *et al.*<sup>27</sup>